High precision radio pulsar timing

Janssen, G.H.

Publication date
2009
Document Version
Final published version

CHAPTER 5

Long-term timing of four millisecond pulsars

G. H. Janssen, B. W. Stappers, C. G. Bassa, I. Cognard, M. Kramer, G. Theureau

Submitted to Astronomy & Astrophysics

Abstract We have timed four millisecond pulsars for up to 10.5 years. The long time span covered makes these pulsars potentially interesting for measuring secular changes in their astrometric parameters, or when in a binary system, constraining the masses of their companions. We provide updates on the timing and flux/intensity properties of four millisecond pulsars, to expand the knowledge of low-mass binary pulsars and solitary millisecond pulsars. Space velocities derived from proper motion measurements of radio pulsars give clues about the evolution of these systems and their birth supernovae. Optical detection and/or characterisation of the white dwarf companions can allow for discrimination between the different types, and with this, constraining their expected masses. Pulsar timing observations were obtained with the Westerbork Synthesis Radio Telescope in The Netherlands, the Nançay Radio Telescope in France and the Lovell telescope at Jodrell Bank in the UK. Archival optical observations were obtained with the ESO 3.6 m telescope at La Silla, Chile. We used standard observing, processing and analysis techniques for the timing and optical observations. We have measured the proper motion for PSRs J1745−0952 and J1918−0642, and we present upper limits for the proper motions of PSRs J1721−2457 and J1810−2005. Using these measurements, in combination with the slowdown rates of the pulsars, we put limits on their space velocities. We present profiles of each pulsar at multiple observing frequencies. We have searched archival optical observations to detect companions of the binary pulsars. However, none were detected. From the scintillation measurements and flux variations

of PSR J1918−0642 we find that the combined effects of refractive and diffractive scintillation give rise to its complex behaviour. The non-detections in the optical observations for PSRs J1745−0952 and J1918−0642 provide lower limits to the mass of their white dwarf companions. Despite having been able to constrain the masses of the pulsar companions from optical observations, and having measured or constrained the proper motions, we were not able to determine for certain whether these sources are low-mass or intermediate-mass binary pulsars. We discuss the possible use of including PSRs J1721−2457 or J1918−0642 in a pulsar timing array.

5.1 Introduction

Millisecond pulsars (MSPs) in low-eccentricity binaries are usually classified as low-mass binary pulsars (LMBPs). They distinguish themselves from intermediate-mass binary pulsars (IMBPs) in having shorter periods (< 10 ms), very low eccentricities ($< 10^{-5}$), and they follow relationships between their orbital period and the eccentricity of their orbit, and their orbital period and the companion mass (Thorsett & Chakrabarty 1999). The origin of the difference between these two classes of binary MSPs is believed to be an evolutionary effect, and mainly due to the progenitor masses of the companion stars. For a low-mass companion ($M_c \lesssim 0.4\,M_\odot$) the mass-transfer during the accretion phase, when the period of the first-born neutron star is being recycled, is believed to be very stable, therefore it can last long enough to lead to very short spin periods (e.g. Phinney & Kulkarni 1994). In contrast, if the companion mass is slightly higher then mass transfer may be more unstable, and will end on shorter timescales leaving a recycled pulsar with spin periods above ∼20 ms. However, there are a few sources which have the properties of both classes where the separation as described above is less clear, e.g. PSR J2145−0750 which has a low eccentricity but a relatively high minimum companion mass (Loehmer et al. 2004), or PSR J0613−0200 that has a higher eccentricity with a low-mass companion (Hotan et al. 2006). There are now ∼65 MSP binary pulsars with probable white dwarf companions known (e.g. Lorimer 2008) and about 16 of these can be regarded as IMBP candidates (Jacoby et al. 2006).

In general, masses of pulsar binary systems are not easy to determine. In some cases, pulsar timing observations on extended timescales with high precision allow for detecting post-Keplerian parameters of the systems, and using those to separately measure the individual masses of the stars. In other cases, optical detection, or failure thereof, of the companion star can be used to derive (limits on) the masses of the system.

Since the discovery of PSRs J1721−2457, J1745−0952, J1918−0642 by Edwards & Bailes (2001), and PSR J1810−2005 by Camilo et al. (2001), no timing update has been published. The three binary pulsars probably qualify as LMBPs, and improving their timing solutions, especially by constraining secular effects like proper motion, is important for statistics on the evolution of these systems. Furthermore, when the masses of the companions to PSRs J1745−0952 or J1810−2005 can be better restricted, they may turn out to be in the IMBP class.

Detecting an optical counterpart to one of the binary pulsars allows properties of their white dwarf companions to be derived. So far, for all three binary pulsars described in this

Chapter, the most recently published limit on optical magnitude of the companion is $R > 24$ (van Kerkwijk et al. 2005).

5.2 Pulsar timing observations and data analysis

5.2.1 Westerbork

The pulsars were observed approximately monthly using the pulsar machines at the Westerbork Synthesis Radio Telescope (WSRT): PuMa (Voûte et al. 2002) since August 1999, and PuMaII (Karuppusamy et al. 2008) since August 2006. The WSRT has three frequency ranges allocated for pulsar timing; for observations centred at 350 MHz we use two bands of 10 MHz wide, and observations centred at 1380 or 2300 MHz use 80 MHz of bandwidth, spread in 8 steps of 10 MHz over a range of 160 MHz. The new pulsar machine uses the full 80 MHz bandwidth at the low frequencies, and all of the available 160 MHz bandwidth at 1380 and 2300 MHz. For all four pulsars presented here, we mainly used the 1380 MHz band as the pulsars were detected in this band, and there are no other reports of detections in other bands. Also this is the best available band for timing at the WSRT. For completeness, we observed all pulsars for one hour at 350 and 2300 MHz, see Fig 5.1.

For a complete description of the PuMa data analysis, we refer to Janssen et al. (2008a). Analysis of the PuMaII data was carried out using the PSRCHIVE (Hotan et al. 2004) software suite. For both instruments, each profile was cross-correlated with a standard profile at the corresponding observing frequency (Fig. 5.1), obtained from the summation of high signal-to-noise (S/N) profiles, to calculate a time of arrival (TOA) for each observation. These were referred to local time using time stamps from a H-maser at WSRT and converted to UTC using global positioning system (GPS) maser offset values measured at the observatory, and GPS to UTC corrections from the Bureau International des Poids et Mesures (BIPM)[1]. The TOAs were converted to the Solar system barycentre using the JPL ephemeris DE405[2]. We used the TEMPO2 timing software package (Hobbs et al. 2006) to analyse the data.

Fluxes were calculated for the WSRT observations by using the aforementioned bandwidth and observing times, the measured S/N ratio for each profile, the gain of the WSRT (1.2 K/Jy), the pulse duty cycle (∼10%), the system temperature and the pulsar specfic radiometer equation (Dewey et al. 1985). The total system temperature was determined from the synthesis data that is taken in parallel with the pulsar observations.

5.2.2 Nançay

PSR J1721−2457, J1745−0952 and J1918−0642 were observed roughly every 3 to 4 weeks with the Nançay Radio Telescope (NRT) since 2006. Equivalent to a 93-m dish, the Nançay Radio Telescope and the BON (Berkeley-Orléans-Nançay) coherent dedispersor were used for typical integration times of 45 min. Coherent dedispersion of a 64 MHz band centred on 1398 MHz is carried out on sixteen 4 MHz channels using a PC-cluster. The Nançay data are recorded on a UTC(GPS) time scale built at the analogue to digital converter by a

[1] http://www.bipm.org [2] ftp://ssd.jpl.nasa.gov/pub/eph/export/DE405/de405iom.ps

Thunderbolt receiver (Trimble Inc.). Differences between UTC and UTC(GPS) are less than 10 ns at maximum, and therefore no laboratory clock corrections are needed. One TOA was calculated from a cross-correlation with a pulse template for each observation of ~ 45 min.

The fluxes for the Nançay data are calculated in a similar way to those for the WSRT except that the system temperature is determined from the known receiver temperature and sky temperature in the direction of the source. The gain of the NRT is 1.4 K/Jy.

5.2.3 Jodrell Bank

PSR J1810−2005 was observed at Jodrell Bank since November 1997, and PSR J1918−0642 since February 2008. Both pulsars were observed every two weeks at a centre frequency around 1400 MHz.

The polarized signals from the receiver were were fed into an analogue filterbank system with $2 \times 32 \times 1$ MHz channels, and filtered and digitised at appropriate sampling intervals and incoherently dedispersed in hardware. The resulting dedispersed timeseries were folded on-line with the topocentric pulsar period and finally written to disc. In the off-line reduction, the two polarisations were summed to form total-intensity profiles. A standard high S/N pulse template was used to determine a TOA for each observation. During this process, TOAs were referred to the local H-maser time-standard and already corrected to UTC using information obtained via the GPS.

5.3 Pulsar timing results and discussion

We present new timing solutions for the pulsars in Table 5.1, based on 7.5 to 10.5 years of radio pulsar timing as described in Sect. 5.2. The vast majority of our timing data were taken using a centre frequency around 1380 MHz, and therefore originally only the observing bandwidth was used to measure the dispersion measure (DM) of the four pulsars. As the combined data sets of WSRT and Nançay or Jodrell Bank together cover more than 200 MHz of bandwidth, the DM was already determined with good accuracy using only that data. However, to allow for refining the DM value even more, and to study the pulse shape and fluxes at other frequencies, we also observed the pulsars at 350 MHz and 2.3 GHz. This resulted in a few detections, see Fig. 5.1. As we have no high S/N templates available at those frequencies, we have used the templates for the pulsars at 1380 MHz to calculate a TOA for those observations in order to include the extra frequencies in the timing solution.

For PSRs J1745−0952, J1810−2005 and J1918−0642, all in very low-eccentricity binaries, we have used the ELL1 timing model (Lange et al. 2001) to avoid the high degree of covariance between the epoch and longitude of periastron.

We have measured significant proper motions for PSRs J1918−0642: $\mu_{\rm T} = 9.2(2)\,{\rm mas\,yr^{-1}}$ and J1745−0952: $\mu_{\rm T} = 24(2)\,{\rm mas\,yr^{-1}}$. By combining those proper motions with the DM-derived distances from the Cordes & Lazio 2002 model, we have calculated transverse velocities for those systems. For the other two pulsars, we use the marginally significant values from the timing solution to calculate a limit on their transverse velocities, see Sect. 5.3.1.

Table 5.1: Timing solutions for pulsars J1721−2457 and J1745−0952. Figures in parentheses are the nominal 1σ TEMPO2 uncertainties in the least-significant digits quoted. [a]The DM distances are estimated from the Cordes & Lazio (2002) model. [b] Velocity limits from Eq. 5.1.

Pulsar name	J1721−2457	J1745−0952
Fit and data-set		
MJD range	52076–54799	52076–54776
Number of TOAs	120	113
Rms timing residual (μs)	31.9	20.8
Weighted fit	Y	Y
Reduced χ^2 value	1.05	1.02
Measured Quantities		
Right ascension, α (J2000)	$17^{\rm h}21^{\rm m}05\overset{\rm s}{.}4963(3)$	$17^{\rm h}45^{\rm m}09\overset{\rm s}{.}1348(2)$
Declination, δ (J2000)	$-24°57'06\overset{''}{.}36(6)$	$-09°52'39\overset{''}{.}682(15)$
Pulse frequency, ν (s^{-1})	285.989343507338(15)	51.609431233273(5)
First derivative of pulse frequency, $\dot{\nu}$ (s^{-2})	$-4.533(5)\times10^{-16}$	$-2.4627(13)\times10^{-16}$
Dispersion measure, DM ($cm^{-3}pc$)	48.34(3)	64.27(9)
Proper motion in RA, μ_α (mas yr^{-1})	1.8(1.8)	−21.2(1.1)
Proper motion in DEC, μ_δ (mas yr^{-1})	−14(25)	11(5)
Binary	–	ELL1
Orbital period, $P_{\rm b}$ (d)		4.943453386(12)
Projected semi-major axis of orbit, x (lt-s)		2.378599(5)
TASC (MJD)		53198.621445(3)
EPS1 (ϵ_1)		0.000009(3)
EPS2 (ϵ_2)		−0.000004(4)
Set Quantities		
Epoch of frequency determination (MJD)	53400.0	53200.0
Epoch of position determination (MJD)	53400.0	53200.0
Epoch of DM determination (MJD)	53400.0	53200.0
Derived Quantities		
Orbital eccentricity, $e = \sqrt{\epsilon_1^2 + \epsilon_2^2}$	-	$1.0(0.4)\times10^{-5}$
Omega, $\omega = \arctan(\epsilon_1/\epsilon_2)$ (°)	-	114(28)
Characteristic age, (Gyr)	10.0	3.3
Surface magnetic field strength, (10^8G)	1.4	13.5
Distance[a], (kpc)	$1.285^{+0.148}_{-0.157}$	$1.796^{+0.282}_{-0.263}$
Spin period (ms)	3.49663	19.3763
Spin period derivative	5.55×10^{-21}	9.23×10^{-20}
Mass function, ($M_\odot$)	–	0.000591270(4)
Minimum companion mass, ($M_\odot$)	–	0.11
Total proper motion, $\mu_{\rm T}$ (mas yr^{-1})	15(25)	24(2)
Transverse velocity, $V_{\rm T}$ (km s^{-1})	$< 140^b$	200(50)
Assumptions		
Clock correction procedure	TT(TAI)	
Solar system ephemeris model	DE405	
Model version number	5.00	

Table 5.2: Timing solutions for pulsars J1810−2005 and J1918−0642. Figures in parentheses are the nominal 1σ TEMPO2 uncertainties in the least-significant digits quoted. [a]The DM distances are estimated from the Cordes & Lazio (2002) model. [b] Velocity limits from Eq. 5.1.

Pulsar name	J1810−2005	J1918−0642
Fit and data-set		
MJD range	50757–54796	52094-54814
Number of TOAs	491	152
Rms timing residual (μs)	270.7	2.6
Weighted fit	Y	Y
Reduced χ^2 value	1.01	1.04
Measured Quantities		
Right ascension, α (J2000)	$18^{\rm h}10^{\rm m}58\overset{\rm s}{.}9919(6)$	$19^{\rm h}18^{\rm m}48\overset{\rm s}{.}035270(13)$
Declination, δ (J2000)	$-20°05'08\overset{''}{.}27(14)$	$-06°42'34\overset{''}{.}8636(6)$
Pulse frequency, ν (s^{-1})	30.467142155106(7)	130.7895141841235(6)
First derivative of pulse frequency, $\dot{\nu}$ (s^{-2})	$-1.3684(11)\times10^{-16}$	$-4.39525(17)\times10^{-16}$
Dispersion measure, DM ($cm^{-3}pc$)	241.0(3)	26.554(10)
Proper motion in RA, μ_α (mas yr^{-1})	0(2)	−7.20(10)
Proper motion in DEC, μ_δ (mas yr^{-1})	17(37)	−5.7(3)
Binary	ELL1	ELL1
Orbital period, $P_{\rm b}$ (d)	15.01201911(4)	10.9131777486(12)
Projected semi-major axis of orbit, x (lt-s)	11.977880(18)	8.3504716(4)
TASC (MJD)	53195.528458(4)	53402.53135510(8)
EPS1 (ϵ_1)	0.000009(3)	−0.00001244(9)
EPS2 (ϵ_2)	−0.000017(3)	−0.00001555(9)
Set Quantities		
Epoch of frequency determination (MJD)	53200.0	53400.0
Epoch of position determination (MJD)	53200.0	53400.0
Epoch of DM determination (MJD)	53200.0	53400.0
Derived Quantities		
Orbital eccentricity, $e = \sqrt{\epsilon_1^2 + \epsilon_2^2}$	$1.9(4)\times10^{-5}$	$1.991(13)\times10^{-5}$
Omega, $\omega = \arctan(\epsilon_1/\epsilon_2)$ (°)	152(12)	218.6(4)
Characteristic age, (Gyr)	3.5	4.7
Surface magnetic field strength, (10^8G)	22.4	4.4
Distance[a], (kpc)	$3.976^{+0.394}_{-0.456}$	$1.230^{+0.127}_{-0.129}$
Spin period (ms)	32.8222	7.64587
Spin period derivative	1.47×10^{-19}	2.57×10^{-20}
Mass function, ($M_\odot$)	0.00818737(4)	0.0052494438(8)
Minimum companion mass, ($M_\odot$)	0.28	0.24
Total proper motion, $\mu_{\rm T}$ (mas yr^{-1})	17(37)	9.2(2)
Transverse velocity, $V_{\rm T}$ (km s^{-1})	$< 400^b$	54(7)
Assumptions		
Clock correction procedure	TT(TAI)	
Solar system ephemeris model	DE405	
Model version number	5.00	

Table 5.3: Contributions to the period derivative. Contributions due to accelerations in the Galactic potential, $\dot{P}_{\rm Gal}$, are calculated using equations in Toscano et al. (1999).

PSR	$\dot{P}_{\rm obs}$	$\dot{P}_{\rm Shk,max}$	$\dot{P}_{\rm Gal,\perp}$	$\dot{P}_{\rm Gal,\parallel}$
J1721−2457	5.55×10^{-21}	2.5×10^{-21}	4.0×10^{-23}	4.4×10^{-22}
J1745−0952	9.23×10^{-20}	4.9×10^{-20}	4.5×10^{-22}	2.8×10^{-21}
J1810−2005	1.47×10^{-19}	5.4×10^{-20}	1.1×10^{-23}	1.8×10^{-20}
J1918−0642	2.57×10^{-20}	1.9×10^{-21}	1.4×10^{-22}	3.7×10^{-22}

5.3.1 Proper motion and velocity

We use our proper motion measurements to derive transverse velocities, or limits on those, for all four pulsars (see Table 5.1). We have a very good measurement of the proper motion of PSR J1918−0642, and a significant detection for PSR J1745−0952. The proper motion values as presented for the other two pulsars are not significant. We note that, although both PSR J1721−2457 and J1810−2005 have ecliptic latitudes very close to the ecliptic plane ($\beta = -1\overset{\circ}{.}8$ and $3\overset{\circ}{.}3$ respectively), and therefore their proper motions may be more easily measured in ecliptic parameters, however, fits in this coordinate system did not result in an improvement of the limits on their proper motions, or the significance of their positions. As both of these pulsars lie quite close to the ecliptic, it may be that they will show effects due to the solar wind (You et al. 2007b). However at the present timing precision we see no influence on the observed TOAs.

Due to changes in the projected line of sight, transverse motions of pulsars can affect observed periodicities in the system (Shklovskii 1970). We present the contributions to the spin period derivative of each pulsar in Table 5.3. For completeness, the contributions to the observed $\dot{P}$ from accelerations in the Galactic potential are also presented, although those are not important effects for these pulsars. To calculate the magnitude of the Shklovskii term we have used the total proper motion values as presented in Table. 5.1. For PSR J1918−0642, the contribution to its spin period derivatives, $\dot{P}_{\rm Shk}$, from proper motion is less than 8% of the observed value. However for PSR J1745−0952, the effect can be as large as 50% of the observed value, leading to an underestimation of the characteristic age and the magnetic field. Moreover, as the proper motions for the solitary pulsar J1721−2457 and PSR J1810−2005 have not been determined significantly yet, the Shlovskii term may even completely dominate the observed $\dot{P}$ for those pulsars. To calculate an upper limit for the proper motion, and accordingly a limit to the transverse velocity, we can use the observed $\dot{P}$ as a maximum:

$$\left(\frac{\dot{P}}{P}\right)_{\rm Shk} < \left(\frac{\dot{P}}{P}\right)_{\rm Obs} . \tag{5.1}$$

This yields $\mu_{\rm T} < 23\,{\rm mas\,yr^{-1}}$ and $V_{\rm T} < 140\,{\rm km\,s^{-1}}$ for PSR J1721−2457 and $\mu_{\rm T} < 22\,{\rm mas\,yr^{-1}}$ and $V_{\rm T} < 400\,{\rm km\,s^{-1}}$ for PSR J1810−2005.

About 50% of the known solitary and low-eccentricity binary pulsars have measured transverse velocities (Tables 2 and 4 in Lorimer 2008). Hobbs et al. (2005) quote mean val-

ues of 2D speeds of 77(16) km s^{-1} for solitary MSPs and 89(15) km s^{-1} for binary MSPs. Compared to those, the (limits on) transverse velocities that we have derived from the proper motion measurements represent normal velocities for recycled pulsars.

5.3.2 Profiles

Apart from our normal timing observing frequency of 1380 MHz, we have observed all four pulsars at additional frequencies: 350 MHz and 2300 MHz. The results are shown in Fig. 5.1. It is now standard procedure for WSRT timing observations of MSPs to use both pulsar machines, and as we have twice the bandwidth available in PuMaII, we present the profile of the detected pulsars at 350 MHz and 2.3 GHz from that data, see Fig. 5.1. Single observations of 55 min. were used to generate the profiles at 350 and 2300 MHz. Where no profile is plotted, the pulsar was not seen at that frequency. The profiles at 1380 MHz were generated using one year of regular timing observations and consist of 10 to 12 observations of 25 min, except for PSR J1918−0642, where again one observation of 55 min. was used. PSR J1745−0952 was detected with NRT at 2600 GHz in an observation of 50 min.

As reported by Kramer et al. (1998), for most MSPs there is very little development of pulse profiles with frequency, which can explained by MSPs having a very compact magnetosphere. For all pulsars except PSR J1810−2005, we indeed see no changes in the pulse profile with changing frequency, except for changes in the ratios of the heights of some components, within the significance of our detections. Compared to its profile at 1380 MHz, the 2300 MHz profile of 1810 appears to have more components in the main peak, and a leading component about 70 degrees before the main peak. Of all the MSP profiles presented by Kramer et al. (1999a) none show more complex profiles at higher frequencies than at lower frequencies. Thus a further study of the profile of PSR J1810−2005 and its polarisation properties could reveal more about MSP emission profiles. The extra features in the peak of the high-frequency profiles of PSR J1810−2005 could be an indication that the profile at 1380 MHz suffers from scattering effects. However, the Cordes & Lazio (2002) model predicts very little scattering for this pulsar at both 1380 MHz (0.26 ms) and 2300 MHz (0.03 ms) suggesting that the features in the pulse profile are intrinsic to the pulsar. It may turn out that, when better sensitivity can be achieved at higher frequencies, PSR 1810−2005 will give better timing results compared with the more commonly used 1380 MHz as its profile shows more features at higher frequencies.

Useful for pulsar timing array?

A very interesting and important use of timing a large set of MSPs to high precision, is the formation of a pulsar timing array (PTA, e.g. Hobbs et al. 2008; Janssen et al. 2008b). Although PSR J1721−2457 is very stable in its timing solution, all values are consistent with the original timing solution as published by Edwards & Bailes (2001), the wide profile of this pulsar does not allow for the high timing precision that is required for PTA pulsars (Jenet et al. 2005).

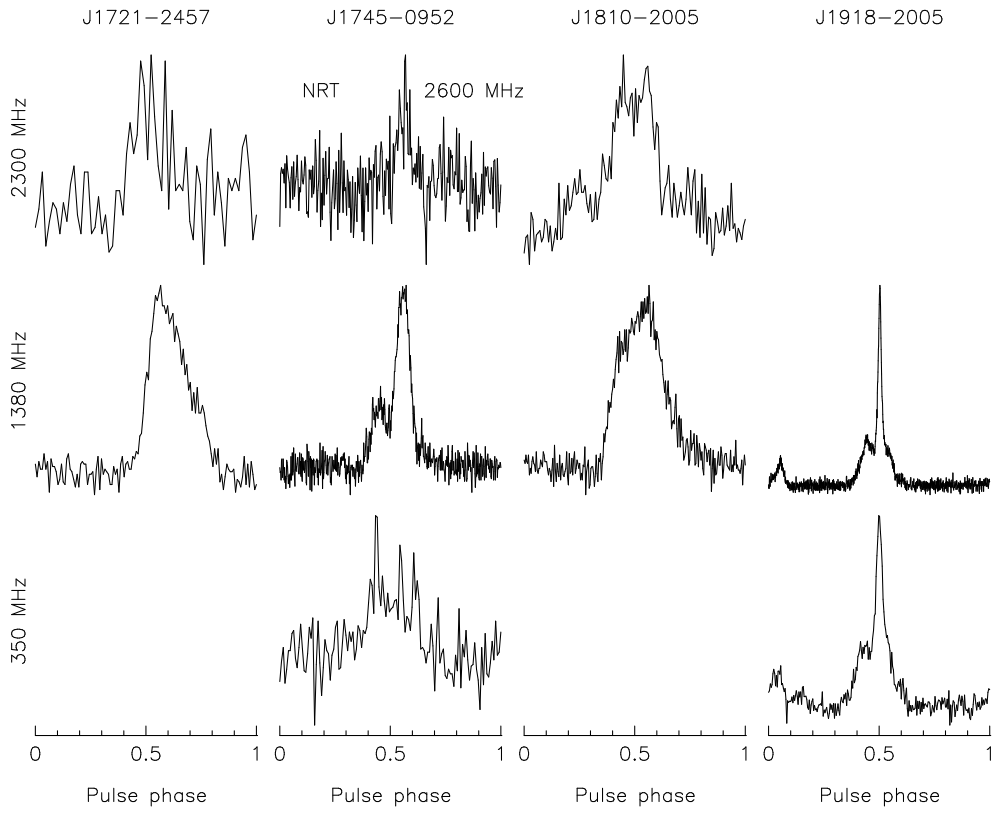

Figure 5.1: Profiles for the PSRs at multiple frequencies. All profiles were generated from a single 55 min. observation using PuMaII, except the 1380 MHz profiles of PSRs J1721−2457, J1745−0952 and J1810−2005 that used 10 to 12 hours of PuMaII observations, and the 2600 MHz profile of PSR J1745−0952 was generated from a 50 min. Nançay observation. These profiles are to show their appearance; for timing purposes we used high S/N templates as described in the text.

In contrast, despite its relatively long spin period compared to most pulsars considered for PTA studies, PSR J1918−0642 may be worthwile to include. Already at 1380 MHz the profile has a very sharp peak, allowing for very precise timing over 7.5 years (rms = 2.3 μs). The pulse profile as shown in Fig. 5.1 was generated by the PuMaII machine in WSRT, promising even better timing precision in the ongoing timing program. Furthermore, it is possible that better results for pulsar timing arrays may be deduced by including not only the best-timing pulsars, but extending the PTA pulsar set with pulsars that have timing solution with rms $\sim$ 1 μs (Jenet et al. 2005; van Haasteren et al. 2008). For PSR J1918−0642, this precision should be reachable using PuMaII timing within the next few years.

Table 5.4: Flux densities and spectral index. These numbers correspond to the profiles in Fig. 5.1. Measurements of flux densities at 350 and 2273 MHz, and PSR J1918−0642 at 1380 MHz are based on one or two 50 min. observations. The ranges in flux densities, and consequently, SI calculations, are now based on the uncertainties in duty cycles.

PSR	S_{350} (mJy)	S_{1380} (mJy)	S_{2273} (mJy)	SI
J1721−2457		0.563-0.596	0.244-0.308	-1.5(2)
J1745−0952	1.524-2.153	0.355-0.414		-1.14(12)
J1810−2005		1.317-1.345	0.825-1.776	0.0(7)
J1918−0642	5.299-6.231	0.562-0.600		-1.67(6)

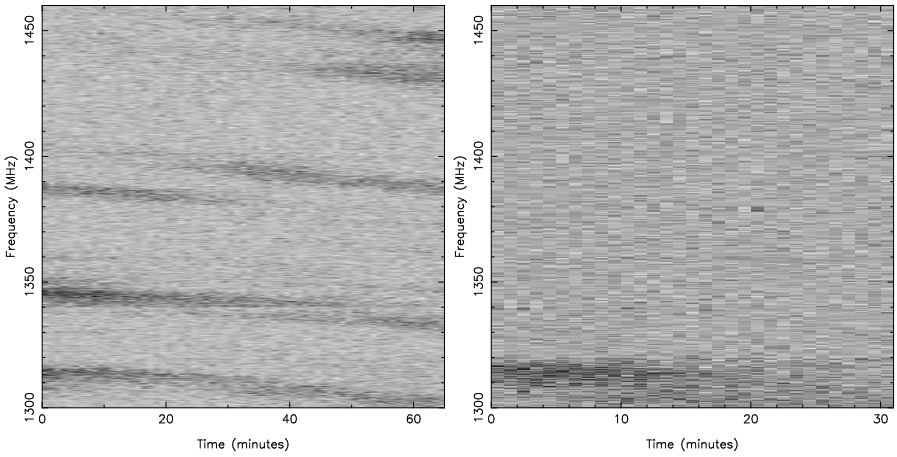

Figure 5.2: Dynamic spectra of PSR J1918−0642 plotted as a greyscale of intensity as a function of time and frequency. Darker pixels correspond to higher intensity values and the intensity scales linearly with the levels of grey. The dynamic spectra are from two observations made using PuMaII on 23 February 2008 (left) and 24 March 2008 (right).

5.3.3 Fluxes and scintillation

We calculated fluxes for the four pulsars, based on the profiles as shown in Fig. 5.1, see Table 5.4. We note that apart from those at 21 cm, the profiles are generated from single observations only, and therefore the resulting flux densities should not be regarded as accurate measurements, but are indicative of the intensities of the pulsars at the observed frequencies. The spectral indices for these pulsars are normal except for PSR J1810−2005, which appears to have a relatively flat spectrum. We observed this pulsar twice at 2.3 GHz, and the resulting fluxes were different by a factor 2, indicating that the brightness of this pulsar may be affected by scintillation.

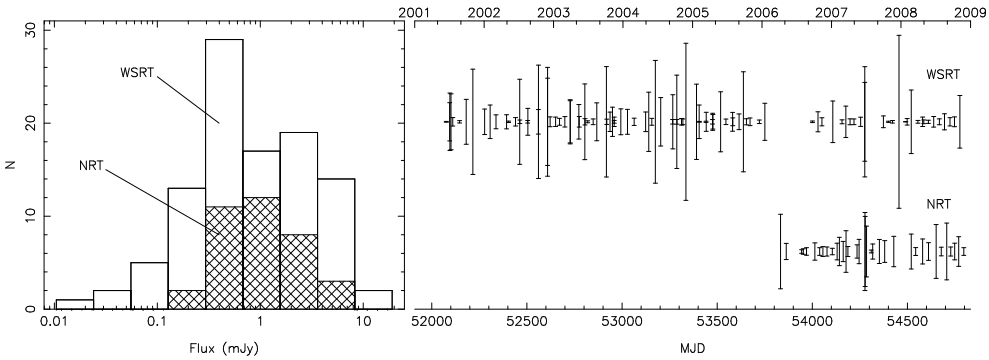

Figure 5.3: Flux variations of PSR J1918−0642 obtained with the WSRT and NRT from observations made at 21 cm. The left panel shows the distribution of fluxes from the two observatories. In the right panel we show the individual flux values as a function of time, where the length of the line in each case is proportional to the flux. Observations where there was no clear detection of the pulsar and thus only and upper limit on the flux can be determined, are not plotted.

Not long after we began our observations of PSR J1918−0642 we noticed that there were a number of occasions when we either did not detect the pulsar at all or it was extremely bright. A plot of the fluxes determined from all observations is shown in Fig. 5.3, noting that this figure does not include observations where the pulsars was not detected at all. The degree of variability is very large, and initially we attributed that to scintillation. However, even with the relatively narrow bandwidth of the PuMa observations, for the dispersion measure of this pulsar the scintillation bandwidth seemed too wide for it to be diffractive scintillation and suggested that it was perhaps refractive (Rickett 2001). When the WSRT fluxes were combined with those from the NRT data the picture became less clear as there were significant differences in the fluxes at the two telescopes, both at sufficiently nearby frequencies as well as on timescales that were too short for refractive scintillation. We have not found any clear correlation with these flux variations on either an orbital or yearly timescale.

Using the improved bandwidth of our PuMaII measurements we were able to better explain the scintillation properties of PSR J1918−0642. In Fig. 5.2 we show the dynamic spectra from two observations of PSR J1918−0642, separated by just one month. The left hand side shows a classic case of scintillation with a scintillation bandwidth of approximately 5 MHz. In contrast, the right hand plot shows just a single scintle, which is perhaps somewhat broader than 5 MHz, across the full 160 MHz of bandwidth. This suggests that the highly variable nature of the flux of this pulsar is due to the refractive modulation of the diffractive interstellar scintillation (Gupta et al. 1994). While beyond the scope of this Chapter, the techniques outlined by Gupta et al. (1994) could be used to further examine the relationship between the velocities in this system and the interstellar medium along the line of sight. We note also that very wide bandwidth observations of this pulsar provide the best opportunity to do high precision timing, as when the pulsar is bright it can be timed to high precision.

5.4 Optical observations

We have analysed archival observations of PSR J1745−0952 and PSR J1810−2005. These observations were obtained with the ESO Multi-Mode Instrument (EMMI) at the 3.6 m telescope of the European Southern Observatory at La Silla, Chile on March 15th, 2004. The instrument has two 2K×4K detectors with $0\farcs166\,\mathrm{pix}^{-1}$ pixels, though these observations were taken with 2×2 binning. The observations consisted of two 10 min. *R*-band exposures of PSR J1745−0952 and two 5 min. *R*-band exposures for PSR J1810−2005. For both pulsars, these long exposures were preceded by short (10 s) exposures, also in the *R*-band. The seeing during these observations was about $0\farcs86$ to $0\farcs88$. All images were bias-subtracted and flat-fielded using twilight flats. The two deep images of each pulsar were averaged and used for further analysis.

The short 10 s observations were astrometrically calibrated against the 2nd version of the USNO CCD Astrograph Catalog (UCAC2, Zacharias et al. 2004). For the PSR J1745−0952 observations, 34 UCAC2 stars overlapped with the chip on which the pulsar was located, of which 26 were not saturated and appeared stellar and unblended, giving rms residuals of $0\farcs056$ in right ascension and $0\farcs091$ in declination. A secondary astrometric catalog was created from the stars on the short exposure and used to calibrate the average of the two 10 min. exposures. For the transfer, about 300 stars were used, giving residuals of $0\farcs022$ in right ascension and $0\farcs025$ in declination. Combined with the uncertainty on the timing position of the pulsar, the quadratic uncertainty of the pulsar position on the deep optical image is $0\farcs060$ in right ascension and $0\farcs096$ in declination. For PSR J1810−2005, we used 23 of the 32 overlapping UCAC2 stars, giving rms residuals of $0\farcs049$ in right ascension and $0\farcs091$ in declination. The transfer of the secondary catalog to the deeper average of the two 5 min. 180 secondary standards, giving residuals of $0\farcs028$ in right ascension and $0\farcs018$ in declination. The final uncertainty on the pulsar position on the deep image is $0\farcs058$ in right ascension and $0\farcs220$ in declination. No sources are present in the error circles of both pulsars, as shown in Fig. 5.4.

In order to determine upper limits on the brightness of the pulsar companions, we performed PSF photometry on the averaged deep images using DAOPHOT II (Stetson 1987). The resulting instrumental magnitudes were calibrated against 47 standard stars in the PG 1525−071 using the calibrated magnitudes of Stetson (2000). Since only *R*-band observations were taken, only the zeropoint was fitted for the calibration, giving rms residuals of 0.02 mag. The standard La Silla *R*-band extinction of 0.07 mag per airmass was used to correct for extinction between the standard observations taken at an airmass of 1.08 and the pulsar observations taken at an airmass of 1.34 (for PSR J1745−0952) and 1.25 (for PSR J1810−2005). Based on the magnitudes and uncertainties of faint stars in the images, we estimate the 3σ detection limit at $R > 24.49$ for PSR J1745−0952 and $R > 24.02$ for PSR J1810−2005.

5.4.1 Model predictions

Though no optical counterparts to PSR J1745−0952, PSR J1810−2005 and PSR J1918−0642 ($R > 24$, see van Kerkwijk et al. 2005) were detected, it is still worthwhile to compare the

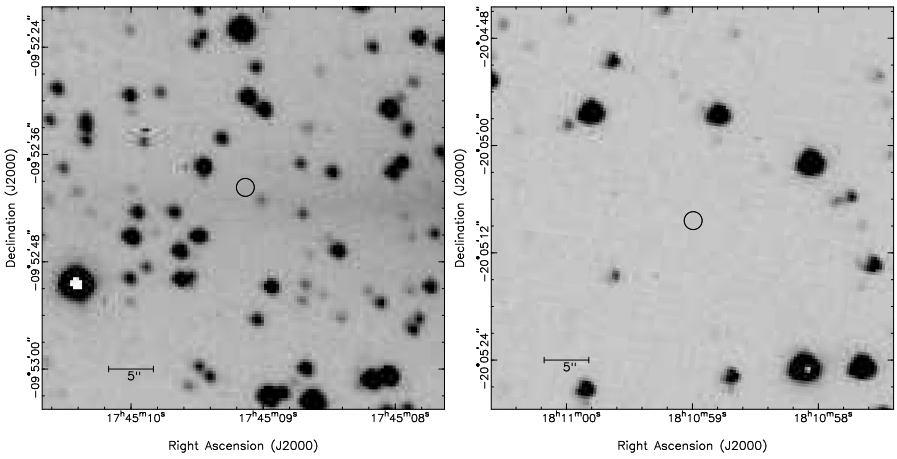

Figure 5.4: 45″ × 45″ subsections of the deep images of PSR J1745−0952 *(left)* and PSR J1810−2005 *(right)*. To retain visibility, the pulsar positions are denoted by a circles with a 1″ radius, even though the actual error ellipses are considerably smaller than this.

upper limits on the white dwarf magnitudes with those predicted by models. To convert the upper limits on the apparent magnitudes to limits on the absolute magnitude, we need estimates for the distance and absorption. Estimates for the distance to each pulsar using the observed dispersion measure and the Cordes & Lazio (2002) model for the Galactic distribution of electrons are given in Table 5.1. The V-band absorption A_V along the line-of-sight and at the distance of each pulsar was estimated using the Drimmel et al. (2003) model for Galactic extinction and converted to R-band absorption A_R using the extinction coefficients of Schlegel et al. (1998) ($A_R = 0.819A_V$). We estimate upper limits on the absolute R-band magnitude of $M_R > 11.3$ for PSR J1745−0952, $M_R > 3.3$ for PSR J1810−2005 and $M_R > 12.7$ for PSR J1918−0642.

In Fig. 5.5 we show predictions of absolute magnitude and cooling ages from the white dwarf cooling tracks by Rohrmann et al. (2002) and Bergeron et al. (1995). The helium-core white dwarf cooling tracks show a dichotomy in the cooling properties of helium-core white dwarfs caused by differences in the thickness of the hydrogen layer surrounding the helium core of these white dwarfs (see, e.g. Schönberner et al. 2000; Althaus et al. 2001). White dwarfs heavier than 0.18–0.20 $M_\odot$ have thin envelopes and cool faster than lighter white dwarfs which have thick envelopes. Cooling tracks appropriate for heavier carbon-oxygen white dwarfs with hydrogen-rich atmospheres are even fainter.

Under the assumption that the characteristic pulsar ages are equal to the white dwarf cooling ages, we plot the upper limits on our white dwarf pulsar companions and detections of others in Fig. 5.5. Because of the large distance and absorption towards PSR J1810−2005, the limit does not constrain any white dwarf parameters. For PSR J1745−0952 and PSR J1918−0642 the upper limits exclude white dwarfs with thick hydrogen envelopes. As such, the mass of the white dwarf in these systems is constrained to $M_c \gtrsim 0.2\,M_\odot$.

For PSR J1745−0952 this mass limit, combined with the low mass function of the system, constrains the inclination of the binary orbit to the low value of $i < 34°$ (assuming $M_{\rm psr} = 1.35\,{\rm M}_\odot$). Should this pulsar have a carbon-oxygen white dwarf, which is not excluded by the optical observations, the limit on the inclination will be even lower.

5.5 Conclusions

Using the WSRT, NRT and Lovell telescopes, we have timed four MSPs for 7.5 to 10.5 years. We have presented updated timing solutions, pulse profiles at multiple frequencies for each pulsar, and scintillation parameters for PSR J1918−0642. We have measured transverse velocities for PSRs J1745−0952 and J1918−0642, and set limits to the velocities of PSRs J1721−2457 and J1810−2005. All velocities are consistent with previously published distributions for solitary and binary MSPs.

We have analysed archival optical observations for the binary MSPs and found no companions to the pulsars. From the magnitde limits we deduce for the companions, we can exclude white dwarfs with thick atmospheres. This indicates that the companions must be heavier than about $0.2\,{\rm M}_\odot$.

For low-eccentricity binary pulsars, the only post-Keplerian parameter that is likely to be measurable is the Shapiro delay. The upper limit for inclination of PSR J1745−0952, i<34 , suggests that the effect of Shapiro delay in timing will be very low and therefore we can not expect to use pulsar timing analyis to disentangle the individual masses of this system. However, the expected luminosity of $M_R > 11.3$ indicates that using a dedicated optical observation, the companion of this pulsar may be detectable, and this will therefore be the most promising way of deducing the pulsar and companion masses.

At this point, the mass restrictions as well as the optical magnitude limits give no conclusive information to classify PSRs J1745−0952 or J1810−2005 as either LMBPs or IMBPs.

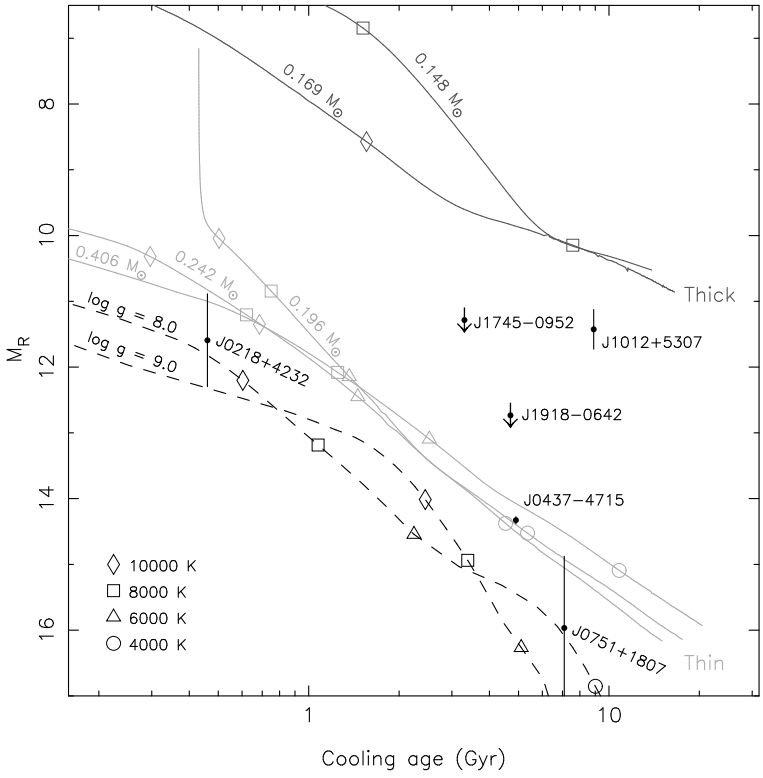

Figure 5.5: Absolute *R*-band magnitude and cooling age predictions. Shown are helium-core white dwarf cooling tracks by Rohrmann et al. (2002) and carbon-oxygen white dwarf cooling tracks with hydrogen-rich atmospheres by Bergeron et al. (1995) ($\log g = 8$ corresponds to $M_c \approx 0.6\,M_\odot$ while $\log g = 9$ corresponds to $M_c \approx 1.2\,M_\odot$). Helium-core models with masses below approximately 0.18–0.20 $M_\odot$ have thick hydrogen envelopes and continue to residually burn hydrogen, keeping the white dwarf hot and slowing the cooling. Heavier models have thin hydrogen envelopes and cool much faster, creating a dichotomy in the cooling properties of white dwarf companions to millisecond pulsars. White dwarfs with carbon-oxygen cores cool even faster. Shown with error bars are PSR J0218+4232 (Bassa et al. 2003), PSR J0437−4715 (Danziger et al. 1993), PSR J0751+1807 (Bassa et al. 2006) and PSR J1012+5307 (Lorimer et al. 1995), where the white dwarf cooling age is assumed to be equal to the characteristic age of the pulsar (using braking indices of $n = 3$). Shown with upper limits on the absolute *R*-band magnitude are the values for PSR J1745−0952 and PSR J1918−0642. For these two pulsars, thick hydrogen envelopes are excluded, indicating the white dwarf companions in these systems are heavier than about 0.2 $M_\odot$.